

PAPER • OPEN ACCESS

## Numerical modelling of failure on brick masonry strengthened with FRCM overlays

To cite this article: João A P P Almeida *et al* 2019 *IOP Conf. Ser.: Mater. Sci. Eng.* **596** 012026

View the [article online](#) for updates and enhancements.



**IOP | ebooks™**

Bringing you innovative digital publishing with leading voices to create your essential collection of books in STEM research.

Start exploring the **collection** - download the first chapter of every title for free.

# Numerical modelling of failure on brick masonry strengthened with FRCM overlays

**João A P P Almeida, Eduardo B Pereira and Joaquim A O Barros**

ISISE, University of Minho, Department of Civil Engineering, School of Engineering;  
4810-058 Guimarães, Portugal

E-mail: j.almeida@civil.uminho.pt

**Abstract.** The behaviour of masonry elements under in-plane loads can be improved by using strengthening overlays. However, the changes in stiffness of the elements after strengthening may have various effects at the level of the behaviour of the entire structure. Advanced numerical simulations can be a helpful and cost effective strategy to guide the efficient design of strengthening systems. These models should simultaneously show the ability to deal with the complexities associated with the composite behaviour of panels at a smaller scale, and allow the simulation of models that can include the entire structure. A constitutive model for a 3D interface finite element, implemented in a FEM-based computer program, was applied for the simulation of the interfaces between substrate and the Fabric Reinforced Cementitious Matrix (FRCM) overlay. The mechanical behaviour of the interfaces between the different layers of the strengthened masonry elements were obtained from direct shear tests on couplet specimens. Subsequently, these results were used to define the constitutive laws of the interface elements. Finally, the numerical model developed was used to simulate the in-plane structural response of the strengthened masonry specimens.

## 1. Introduction

The use of strengthening techniques based on the application of reinforcing overlays to masonry substrates is widespread. To enhance the tensile behaviour and ductility, different types of materials can be used as reinforcement, in the form of meshes made of steel, polymers, carbon or glass [1,2].

The in-plane behaviour of masonry infill panels gives an important contribution to the strength of structures subjected to horizontal actions. The in-plane characterization of masonry panels can be performed by means of the diagonal tensile test (DTT), using specimens built in the laboratory, [3], or in-situ [4]. Different types of strengthening systems have been evaluated using this type of test [5,6]

Fabric reinforced cementitious matrix systems (FRCM) are considered of great potential, because the increase of ductility can be achieved with simple and economic strengthening procedures. In order to assess the effectiveness of these strengthening systems the in-plane behaviour must be studied [7]. However, these systems often show vulnerability at the level of the interface due to the sharp gradient of mechanical properties between the substrate and the strengthening system [8].

This work discusses the numerical modelling strategy adopted for simulating the in-plane tests carried in unreinforced and strengthened masonry. Further details about the experimental programme, as well as the discussion of the main results obtained, may be found in Almeida et al.[9].

Considering the importance of testing and developing numerical tools for supporting the design process of masonry structures strengthened by FRCM overlays, the numerical strategy adopted was devised trying to achieve the optimum balance between modelling accuracy and computational cost.



### 1.1. Experimental characterization of the in-plane behaviour

As discussed by Almeida et al. in [9], the cyclic effect on the shear behaviour of masonry panels can be characterized by means of DTT's. The contribution of the strengthening effect provided by FRCM overlays to the in-plane structural behaviour under cyclic loading was accessed in specimens with geometry similar to figure 1(a). Cyclic DTT's were carried out by Brignola et al. [4], under force control, considering a load increment of 200 N/s, and at least four cycles for each specimen. Santa-Maria et al. [10] used this type of test but considering a different procedure, which started by the loading and unloading of the first diagonal of the specimen, followed by the loading and unloading of the second diagonal.

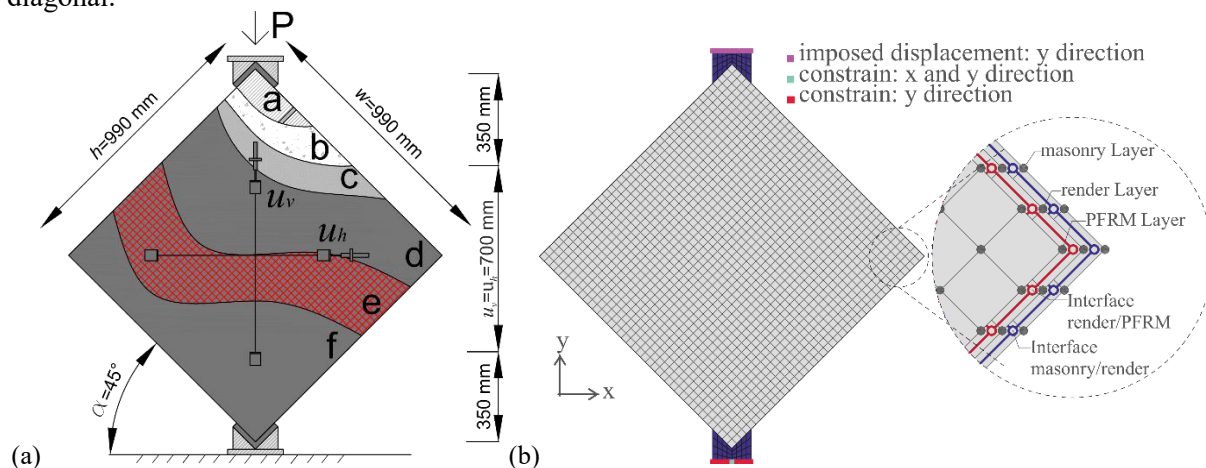


Figure 1. (a) General set-up of a DTT. (a – masonry; b – roughcast mortar; c – render layer of 15 mm thickness; d – Polypropylene fibre reinforced mortar (PFRM) of 12.5 mm thickness; e – carbon fibre mesh; f – PFRM of 12.5 mm thickness.); (b) Finite element model, imposed displacements and constraints, and detail of the layers.

### 1.2. Numerical modelling of in-plane tests

Masonry walls exhibit a complex structural behaviour since masonry is a composite material formed by constituents showing brittle behaviour. Two main numerical approaches have been adopted by researchers to describe the mechanical behaviour of masonry, macro-modelling and micro-modelling [11]. In macro-modelling, masonry is considered as a homogeneous material, while in micro-modelling, masonry is considered as an assembly of units connected by joints. When considering masonry strengthened with overlay systems, two types of approaches can be considered: those that model the behaviour of the strengthening layer and interface in a coupled manner by means of homogenization; approaches that model the masonry, the reinforcement and the interface separately [12]. In the second case interface finite elements with nonlinear constitutive laws are used. The nonlinear behaviour of masonry was reproduced in various studies using a smeared crack approach [3,12]. Typically, the masonry is modelled as an isotropic continuum material before any nonlinear effect, and orthotropic or even anisotropic continuum material after cracking, by adopting constitutive laws for modelling the nonlinear behaviour in tension and compression, and considering also the degradation of shear stiffness and strength with the smeared cracking propagation.

## 2. Materials, test procedures and relevant results

The complete discussion of the experimental program may be found elsewhere ([8,9]).

The specimens presented a square geometry with approximately 990 mm. The thickness was 140 mm for reference and 190 mm for the strengthened specimens. The specimens were assembled using hollow ceramic bricks (Length x Height x Thickness:  $28.5 \times 19.5 \times 11.0$  cm<sup>3</sup>) and cement mortar for the joints. Subsequently a render layer of a cementitious mortar with a thickness of 15 mm was applied on both faces. In the case of the strengthened specimens, after the stages previously described a first layer of polypropylene fibre reinforced mortar (PFRM) with 12.5 mm thickness was applied, then a carbon

fibre mesh was placed over that layer and finally a second layer of PFRM with the same thickness was applied, see figure 1. All materials were characterized experimentally. In the case of the carbon mesh, the mechanical properties were obtained from the supplier, see table 1.

Table 1. Properties of the masonry components, render and FRCM.

Masonry components	
Compressive strength of units, parallel to hollows *	6.55 (8%) N/mm <sup>2</sup>
Compressive strength of units, normal to hollows *	2.21 (9%) N/mm <sup>2</sup>
Compressive strength, mortar joints and render *	8.58 (7%) N/mm <sup>2</sup>
Flexural strength, mortar joints and render *	2.11 (3%) N/mm <sup>2</sup>
Adhesion strength to render layer to brick *	0.51 (22%) N/mm <sup>2</sup>
Polypropylene fibre reinforced mortar	
Density	2050 kg/m <sup>3</sup>
Elasticity modulus, [13]	38240 N/mm <sup>2</sup>
Compressive strength*	36.46 (6%) N/mm <sup>2</sup>
Flexural strength, [13]*	6.25 (5%) N/mm <sup>2</sup>
Adhesion strength to render layer*	1.48 (20%) N/mm <sup>2</sup>
Carbon Fibre Mesh [14]	
Carbon fibres in both directions	50 threads/m
Elasticity modulus	≥240 kN/mm <sup>2</sup>
Tensile strength	≥4300 N/mm <sup>2</sup>
Elongation at rupture	1.75 %
Ultimate tensile force	185 kN/m

\*The values in parenthesis represent the coefficient of variation.

The elasticity modulus of the render,  $E_{ci}$ , was estimated using equation (1), as suggested by the Model Code 2010 [15], considering the compressive strength obtained from compression tests on cylindrical mortar specimens, which resulted in  $E_{co}=20431$  MPa.

$$E_{ci} = E_{co} \times \alpha_E \times \left( \frac{f_{cm}}{10} \right)^{1/3} \quad (1)$$

where:  $E_{co}$  is a constant value ( $21.5 \times 10^3$  MPa);  $\alpha_E$  represents the effect of the type of aggregates (1.0 for quartzite aggregates) and  $f_{cm}$  is the average compressive strength at 28 days (8.58 MPa).

The compressive strength and the elasticity modulus of the masonry weakest direction were deduced considering the provisions of Eurocode 6, [16]. The characteristic compressive strength value,  $f_k$ , may be estimated by equation (2).

$$f_k = K \times f_b^{0.7} \times f_m^{0.3} \quad (2)$$

where:  $k$  is a constant ( $k=0.35$ );  $f_b$  is the normalized mean compressive strength of the brick units in the direction of the applied action effect ( $f_b=2.21$  MPa);  $f_m$  is the compressive strength of the mortar joint, which should not be considered as greater than 20 MPa or greater than  $2f_b$  when units are assembled using general purpose mortar;  $f_m=4.42$  MPa.

Following these assumptions,  $f_k=0.95$  MPa. For estimating the elasticity modulus of masonry,  $E_m$ , Eurocode 6 [16] suggests  $700f_k > E_m > 1000f_k$ , ( $667 > E_m > 952$  MPa). In this case,  $E_m=952$  MPa was adopted, once more isotropic behaviour was assumed.

The load vs displacement responses obtained for the reference and the strengthened specimens are presented in figure 4. The vertical and horizontal displacements represent the average of the measurements obtained from a pair of LVDT's placed in opposite sides of the specimens. The strengthened specimens, FRCM\_EXP, have reached considerably higher strength than the reference specimens, REF\_EXP. The load vs displacement responses obtained for the strengthened specimens

presented, in general, a low scatter of results. Besides the increase of the pre-peak load carrying capacity observed, the peak loads were reached for higher displacements than the ones registered for the reference specimens. After reaching the peak load the strengthened specimens presented a relatively smooth load decay with the increase of the horizontal deformation.

### 3. Characteristics of the Finite Elements models

#### 3.1. Finite element mesh and boundary conditions

The finite element analysis was carried out using the computer code FEMIX 4.0 [17]. All the nonlinear static analyses were performed using the Newton–Raphson iteration method. The numerical simulations used a macro-modelling approach, where the masonry and the FRCM layers were considered as continuum materials. Due to symmetry conditions, the model was simplified, only one half of the specimen was discretized along the direction of the thickness. Consecutive material layers were connected by interface elements. The simulation of each material layer was done through the Reissner–Mindlin theory adapted to layered shells [18]. Finite elements of 4 nodes and 2x2 Gauss-Legendre integration points were used in the numerical model, figure 1(b). Surface interface Lagrangian finite elements of 8-node with 2 integration points in each direction were adopted to simulate the interfaces between different layers (masonry/render and render/FRCM). Finite elements of 25x25 mm<sup>2</sup> were used for all the layers and interfaces. All rotations were kept free.

#### 3.2. Masonry, render and FRCM overlay constitutive models

The contribution of microfibres present in the mortar matrix and the strengthening carbon mesh for the post-cracking behaviour of the FRCM strengthening overlay was simulated in the smeared cracking model by using a softening law exclusively for fracture mode I, figure 2(a), since their effect in fracture mode II was assumed of marginal impact [19]. The tension-softening or tension-stiffening behaviour of materials can be simulated by changing the normalized coordinates ( $\xi_i$ ;  $\alpha_i$ ) that define the transition points of the diagram, the tensile strength,  $f_{ct}$ , and the mode I fracture energy,  $G_f^I$ . The ultimate crack strain,  $\varepsilon_{n,u}^{cr}$ , is defined as a function of the parameters  $\alpha_i$  and  $\xi_i$ , the mode I fracture energy, the tensile strength, ( $\sigma_n^{cr} = f_{ct}$ ), and the crack bandwidth,  $l_b$  [20]. The crack bandwidth aims to guarantee that the results are mesh objective [21].

In the case of the masonry and of the render, a smeared cracking approach was also used to simulate their post-cracking behaviour. However, the quasi-brittle behaviour of both the masonry and the render in tension, is better simulated by adopting a bilinear law, or the Cornelissen softening law, having this last one been adopted. The Cornelissen's softening law simulates the tension-softening behaviour by considering an exponential function for the crack opening vs tensile strength [22]. The parameters used in the constitutive model were the tensile strength,  $f_{ct}$ , the mode I fracture energy,  $G_f^I$ , and the crack bandwidth,  $l_b$ , as shown in figure 2(b).

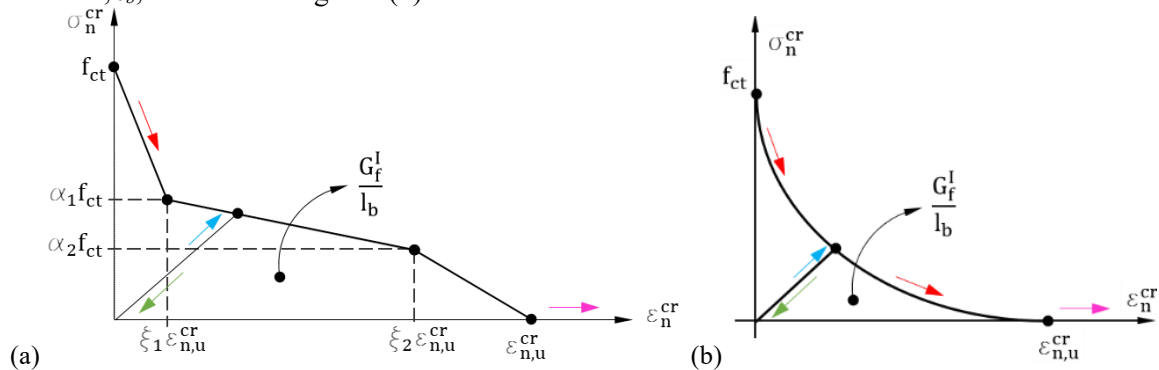


Figure 2. Diagrams for modelling the fracture mode I component of crack constitutive law of the multi-directional smeared crack model [20]: (a) Trilinear diagram; (b) Cornelissen's diagram. (Colour legend for crack status: red-opening; green – closing; dark blue-closed; light blue-reopening; cyan-fully open.).

### 3.3. Constitutive model for the surface interface finite elements

Both the interfaces between the masonry and the render, and between the render and the FRCM layers have been simulated by following a discontinuous strategy based on the adoption of the surface interface finite elements represented in figure 3(b). The constitutive model (CM) is governed by the yield function ( $f$ ) and the yield surface gradient ( $n$ ), the plastic potential ( $g$ ) and the plastic potential variables ( $\psi$ ), plastic flow direction ( $m$ ), the hardening law ( $\Delta k$ ) and the hardening variables ( $\Phi$ ). Work hardening and non-associated flow were assumed. The yield surface is governed by three hardening variables, which are the tensile strength ( $\chi$ ), the shear strength ( $c$ ) and the friction angle ( $\tan \phi$ ), as shown in equation (3) and figure 3(a).

$$f = f[\sigma_N, \sigma_T] = \sigma_T^2 - (c - \sigma_N \times \tan \phi)^2 + (c - \chi \times \tan \phi)^2 \quad (3)$$

Where  $\sigma_N$  and  $\sigma_T$  represent the normal and tangential stress respectively.

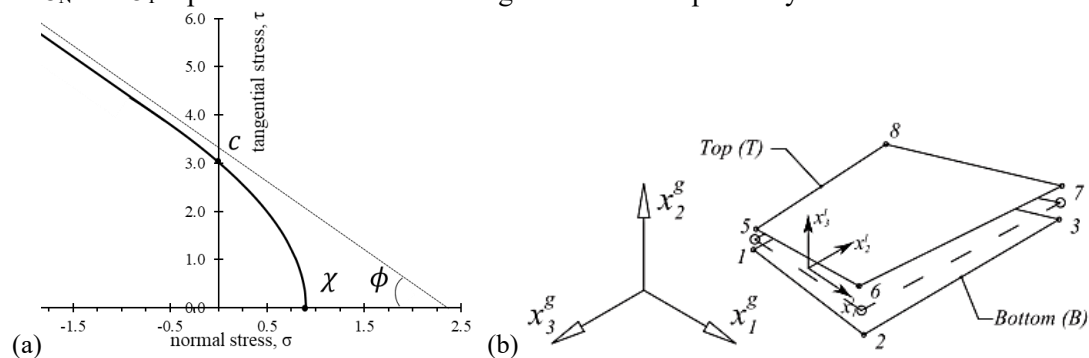


Figure 3. (a) Representation of the Mohr failure criterion when used to characterize the interaction between the normal stress and the peak values for positive tangential stresses. (b) Lagrangian 8-node surface interface element used in the numerical models.

A dilation stress ( $\sigma_{dil}$ ) which corresponds to the normal stress at which the dilatancy vanishes when compression and shear stresses occur at the same time, was also considered in the constitutive model.

The evolution of the yield surface and the evolution of the hardening parameters depend on the evolution of the plastic work ( $W$ ). Additionally, the increase of the plastic work is reflected by means of a dimensionless parameter that is related to the portion of the fracture energy ( $G_f$ ) dissipated. Two dimensionless parameters are associated to the fracture modes I and II. The constitutive model used is designated as CM I/II\_2D by Coelho et al. [23].

## 4. Numerical simulation of the reference prototype

### 4.1. Analysis of masonry and render properties

The tensile strength ( $f_{ct}$ ) of the masonry and of the render were estimated based on the ratio ( $f_{ct}/f_c$ ) equal to 0.10, according to Angelillo et al. [24]. Conversely, the mode I fracture energy of the masonry was considered equal to 0.01 N/mm, taking the results obtained by Basili et al. [12]. The mode I fracture energy of the render layer was calculated following the experimental procedure of RILEM 50-FMC, [25]. A value of 0.12 N/mm with a coefficient of variation of 16% was obtained.

The Cornelissen's softening law was used for both materials. A parametric analysis was carried out to ascertain the sensitivity of the numerical responses obtained with respect to the mode I fracture energy ( $G_f$ ), as well as their approximation to the experimental results. Within the range of values considered, 0.005 to 0.03 for the masonry, and 0.05 to 0.30 N.mm for the render, the parametric analysis shown that the values that better matched the experimental response where 0.02 N.mm for the masonry and 0.20 N.mm for the render.

The mechanical characterization of the interfaces responses was carried out by performing direct shear tests in couplet specimens according to the procedure and set-up presented in Almeida *et al.* [8].



The cohesion and the friction angle values, obtained from the experimental results, were used to define the interface constitutive model, see table 2. Additionally, mode II fracture energy was obtained from the shear stress vs slip experimental responses [8].

The resulting load vs displacement numerical responses are plotted in figure 4. The simulation that showed a better agreement to the experimental results was the REF\_NUM\_03, presenting similar values of the peak-load and a similar post-peak behaviour.

Table 2. Proprieties defining interface behaviour.

Description	Symbol	Units	Interface masonry/render	Interface render/PFRM
Tensile strength	$\chi$	MPa	0.51	1.48
Cohesion in yield function	$c$	MPa	4.8	6.0
Normal stress at which the dilatancy vanishes	$\sigma_{dil}$	MPa	0.1	0.3
Friction angle in yield function	$\tan\phi$	—	0.43	0.80
Residual friction angle	$\tan\phi_r$	—	0.10	0.30
Dilation angle	$\tan\beta$	—	0.05	0.15
Tensile strength softening parameter	$\alpha_\chi$	—	0.5	0.5
Cohesion softening parameter	$\alpha_c$	—	0.5	0.5
Friction angle softening parameter	$\alpha_{\tan\phi}$	—	0.5	0.5
Fracture energy in mode I	$G_f^I$	N/mm	0.01	0.03
Fracture energy in mode II	$G_f^{II}$	N/mm	0.4	0.8
Elastic tangential stiffness in local direction $l_1$	$k_{e1}$	MPa/mm	120	150
Elastic tangential stiffness in local direction $l_2$	$k_{e2}$	MPa/mm	120	150

#### 4.2. Load vs displacement response

The numerical load vs displacement response obtained for the reference specimens is presented in terms of vertical and horizontal displacement between two points of the mesh in the render layer, equivalent to the LVDT's position during testing, see figure 1. The response obtained for the reference model, REF\_NUM\_03, shows a first branch characterized by a linear evolution considering both the horizontal and the vertical displacements. After this phase, two different behaviours can be observed; considering the horizontal displacements, the load vs displacement response is characterized by an increase of the load until the peak load is reached, and the subsequent mild softening, following closely the response obtained experimentally; when considering the vertical displacements.

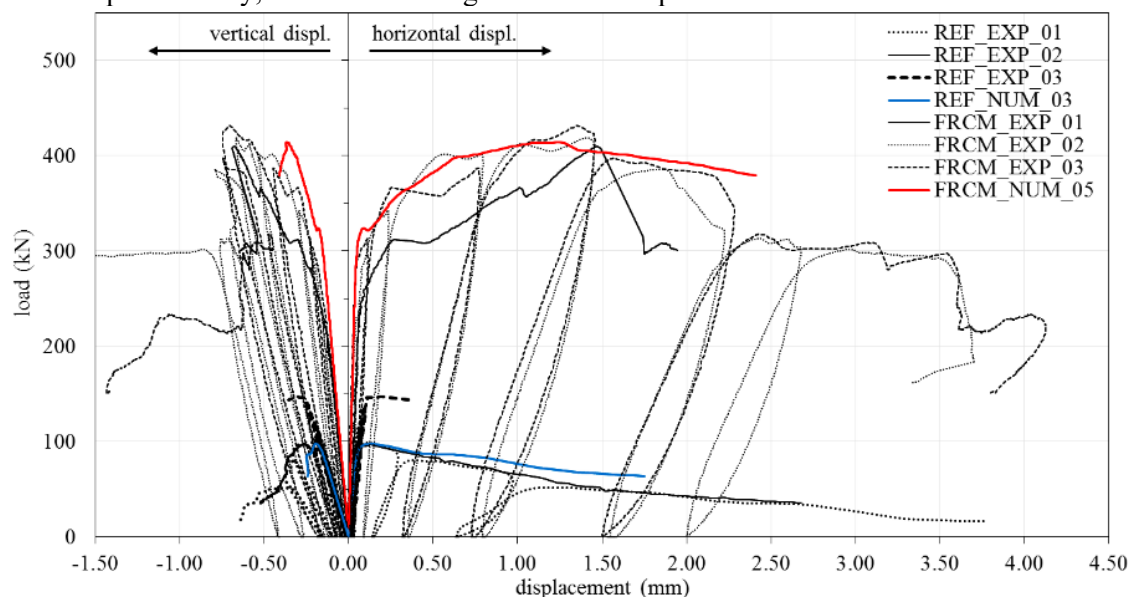


Figure 4. The load vs displacement response of the numerical simulation and experimental results.

## 5. Numerical simulation of the strengthened prototype

### 5.1. Analysis of FRCM properties

The values of the  $f_{ct}$  and of the mode I fracture energy ( $G_I^I$ ) for the FRCM system were estimated considering an effective composite behaviour resulting from the combination of the carbon fibre mesh and of the PFRM. According to the Model Code 2010 [15], the flexural tensile strength ( $f_{ctm,flex}$ ) can be obtained as a function of the axial tensile strength ( $f_{ctm}$ ), resulting in  $f_{ctm}=1.75$  MPa. For mode I fracture energy a sensitivity analysis was carried out considering values between 1.00 N/mm and 2.00 N/mm. Also the shape of the softening diagrams for modelling the crack opening in mode I were analysed. Two different softening diagrams were considered, the ( $\xi_i, \alpha_i$ ) values for each point of the diagrams were assumed taking into account the composite nature of the strengthening system. Diagram 1 was defined by (0.05,0.7;0.6,0.5) and diagram 2 by (0.02,0.6;0.6,0.2) see figure 2(a). For both diagrams three different values of fracture energy were considered, 1.00, 1.25 and 1.50 N/mm. The response considering diagram 2 and fracture energy of 1.25 N/mm, FRCM\_NUM\_05, presents the best agreement with the experimental, see figure 4.

### 5.2. Load vs displacement response

The response registered for the strengthened specimens, FRCM\_NUM\_05, is shown in figure 4. The load-displacement response in terms of the horizontal displacement shows a first linear branch with a slope similar to the experimental, followed by a non-linear phase that also presents a good agreement with the experimental. At the initial part of this phase a local peak occurs, and this behaviour is justified by the steep shape of the first branch of the tensile softening diagram adopted for modelling the crack opening in mode I. When the peak load is reached, both the load and displacement are in agreement with the average experimental values. After the peak, a softening behaviour is observed, where the load response presents a relatively smooth load decay with the increase of the horizontal deformation. For higher deformations the load decays observed in the experimental responses were slightly steeper than the one obtained in the numerical simulation. The load-displacement numerical response considering the vertical displacements also presents a first branch with a slope matching the experimental. After this stage, when the non-linear behaviour begins, an increasing lag between numerical and experimental responses can be observed. This lag reaches approximately 0.3 mm at the peak stage. Probably this difference may be justified by some degree of crushing existing at the interfaces between masonry units, joints and overlays, which is not conveniently simulated by the numerical model since elastic behaviour in compression is considered for the sake of computational efficiency. After the peak, an abrupt decay occurs, and a similar response was observed in the experimental tests.

## 6. Discussion of results

The average shear stress,  $S_s$ , in accordance with the ASTM E519 [26], is obtained by  $S_s = 0.707 P/A_n$ , where  $P$  is the applied load and  $A_n$  is the net area of the section of the panels (96740 mm<sup>2</sup> for reference, and 147778 mm<sup>2</sup> for FRCM model). The average vertical and horizontal strains,  $\varepsilon_v$  and  $\varepsilon_h$  have been computed by dividing the average displacement along the compressive and tensile diagonals, respectively, by the gauge lengths in each case. The shear strain,  $\gamma$ , was finally computed as  $|\varepsilon_v| + \varepsilon_h$ . The obtained shear stress vs shear strain responses are presented in figure 5.

The shear stress, shear strain and modulus of shear stiffness that were obtained for the elastic branch and at peak are presented in table 3. The average peak shear stress deduced from the experimental tests and the one obtained from the numerical simulation differ less than 17% for the reference and less than 1% for the strengthened models. In the case of the modulus of shear stiffness the difference is of 14% and 20% when considering the elastic branch until 1/3 of the peak stress is reached. When considering the peak shear stress values, as recommended by ASTM E519 [26], the differences are respectively 12% and 32%.



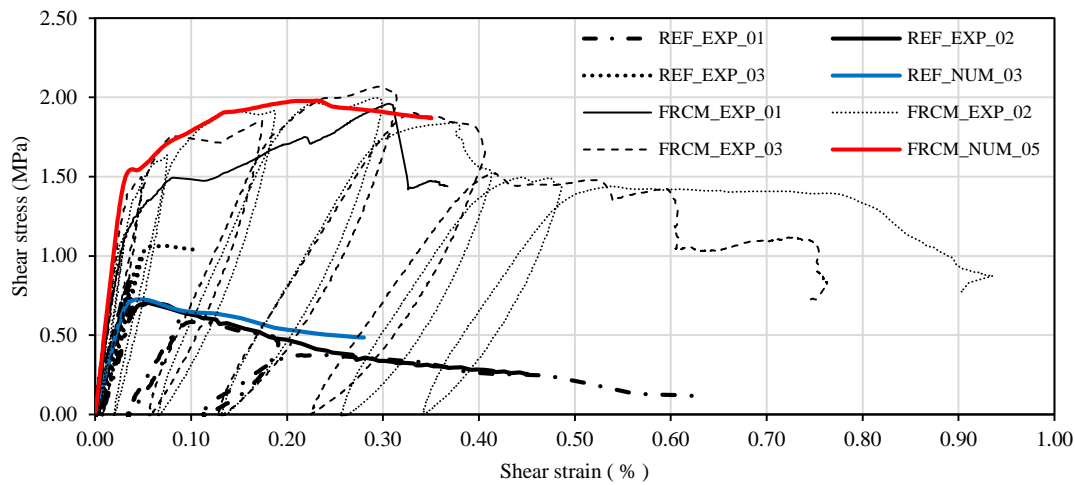


Figure 5. Shear stress vs shear strain response of experimental tests and numerical simulations.

Table 3. Average of the limit values obtained for the experimental and numerical responses.

Response range	Type specimen	of	Shear Stress, $s_s$ (MPa)		Shearing Strain, $\gamma$ (%)		Modulus of shear stiffness, $G$ (MPa)	
			Exp.	Num.	Exp.	Num.	Exp.	Num.
Elastic branch	Reference		0.185	0.186	0.007	0.008	2716	2325
	Strengthened		0.532	0.536	0.012	0.010	4458	5360
Peak	Reference		0.871	0.725	0.054	0.049	1696	1485
	Strengthened		2.002	1.978	0.299	0.231	651	856

The shear stress field at the interface elements between masonry/render and render/FRCM layers for peak load are presented in figure 6. The interface shear stresses are presented for local direction 11. For direction 12 an anti-symmetric shear stress field was obtained. The normal stresses for direction 13, perpendicular to the plane XY, where null in all cases. The shear stresses obtained in the elements for both interfaces are lower than the value of the cohesion adopted for the interface model, see table 2, which demonstrates that the interfacial behaviour remained elastic throughout the entire loading sequence. Nonetheless, for the interface masonry/render it is possible to identify values of shear stress higher than for render/FRCM interface, which indicate that delamination is more likely between the masonry and the render layers. The interfacial stresses do not reach sufficiently high values to produce the interfacial delamination. In contrast, during the experimental testing the delamination was identified. The delamination observed experimentally may have result from possible initial stress states at the interfaces due to shrinkage, which were not were not considered in the numerical model.

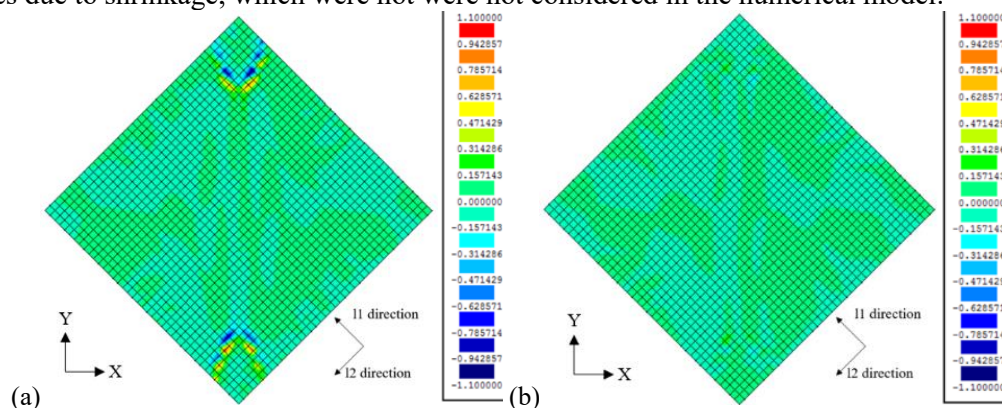


Figure 6. Contour plot of the shear stress (MPa) in interface elements for direction 11: (a) Masonry/Render; (b) Render/FRCM.

## 7. Conclusions

In summary, the numerical simulations of the reference and the strengthened masonry models have produced reasonable and accurate results when compared to the experimental responses, without the need to resource to excessively refined or computationally costly models.

The numerical load-displacement responses have reproduced quite well the experimental ones when the horizontal displacement is regarded. In the case of the experimental load-displacement responses regarding the vertical displacement, the numerical results have shown a general tendency to underestimate the displacements observed experimentally. This is most likely related to the fact that all materials have been assumed to behave linear elastically in compression. However, this effect was not significant and the computational cost was kept lower than if nonlinear behaviour in compression was additionally considered.

The overall shear stress vs shear strain responses obtained from the numerical models have accurately simulated the experimental responses observed, which is particularly interesting for supporting simplified design procedures of the masonry strengthening systems based on the application of FRCM overlays, such as the procedures presented in ACI 549.4R-13 [7].

## Acknowledgements

The first author wishes to acknowledge the grant SFRH/BD/115090/2016, provided by FCT.

## References

- [1] Papanicolaou C G, Triantafillou T C, Karlos K and Papathanasiou M 2007 Textile-reinforced mortar (TRM) versus FRP as strengthening material of URM walls : in-plane cyclic loading *Mater. Struct.* **40** 1081–97
- [2] Corradi M, Borri A, Castori G and Sisti R 2014 Shear strengthening of wall panels through jacketing with cement mortar reinforced by GFRP grids *Compos. Part B Eng.* **64** 33–42
- [3] Milosevic J, Gago A S, Lopes M and Bento R 2013 Experimental assessment of shear strength parameters on rubble stone masonry specimens *Constr. Build. Mater.* **47** 1372–80
- [4] Brignola A, Frumento S, Lagomarsino S and Podestà S 2008 Identification of Shear Parameters of Masonry Panels Through the In-Situ Diagonal Compression Test *Int. J. Archit. Herit.* **3** 52–73
- [5] Dehghani A, Fischer G and Nateghi Alahi F 2013 Strengthening masonry infill panels using engineered cementitious composites *Mater. Struct.* 1–20
- [6] Parisi F, Iovinella I, Balsamo A, Augenti N and Prota A 2013 In-plane behaviour of tuff masonry strengthened with inorganic matrix – grid composites *Compos. Part B* **45** 1657–66
- [7] ACI Committee 549 2013 ACI 549.4R-13: Guide to Design and Construction of Externally Bonded Fabric- Reinforced Cementitious Matrix (FRCM) Systems for Repair and Strengthening Concrete and Masonry Structures (Farmington Hills, Michigan)
- [8] Almeida J A P P, Bordigoni D, Pereira E N B, Barros J A O and Aprile A 2016 Assessment of the properties to characterize the interface between clay brick substrate and strengthening mortar *Constr. Build. Mater.* **103** 47–66
- [9] Almeida J A P P, Pereira E B and Barros J A O 2015 Assessment of overlay masonry strengthening system under in-plane monotonic and cyclic loading using the diagonal tensile test *Constr. Build. Mater.* **94** 851–65
- [10] Santa-Maria H, Duarte G and Garib A 2004 Experimental Investigation of masonry panels externally strengthened with CFRPlaminates and fabric subjected to in-plane shear load *13th World Conference on Earthquake Engineering* (Vancouver, B.C., Canada)
- [11] Lourenço P B 1996 Computational strategies for masonry structures (Delft University)
- [12] Basili M, Marcari G and Vestroni F 2016 Nonlinear analysis of masonry panels strengthened with textile reinforced mortar *Eng. Struct.* **113** 245–58

- [13] Frazão C, Barros J and Gonçalves D Durability of cementitious mortars reinforced with synthetic fibers (in Portuguese) *IIº Encontro Luso-Brasileiro de Degradação de Estruturas de Betão, Lisboa, LNEC, 27-29 de Setembro de 2016*
- [14] S&P Clever Reinforcement Company AG 2013 S&P ARMO-System FRCM Design Guidelines - Fiber Reinforced Cementitious Matrix (VER12.03.2013/IND) (Seween)
- [15] fib - federation internationale du Beton 2013 *fib Model Code for Concrete Structures 2010* (Wiley-VCH Verlag GmbH & Co. KGaA)
- [16] Comité Européen de Normalisation 2005 EN 1996-1-1:1995 Eurocode 6 - Design of masonry structures - Part 1-1: General rules for reinforced and unreinforced masonry structures
- [17] Azevedo A F M, Barros J A O, Sena Cruz J M and Ventura Gouveia 2003 Software in teaching and structures design (in Portuguese) *Proceedings of III Congresso Luso\_Moçambicano de Engenharia* (Mozambique) pp 81–92
- [18] Ventura-Gouveia A, Barros J A O and Azevedo A F M 2011 Crack constitutive model for the prediction of punching failure modes of fiber reinforced concrete laminar structures *Comput. Concr.* **8** 735–55
- [19] Barros J A O, Baghi H, Dias S J E and Ventura-Gouveia A 2013 A FEM-based model to predict the behaviour of RC beams shear strengthened according to the NSM technique *Eng. Struct.* **56** 1192–206
- [20] Sena-Cruz J M 2004 Strengthening of concrete structures with near-surface mounted CFRP laminate strips (University of Minho)
- [21] Edalat-Behbahani A, Barros J A O and Ventura-Gouveia A 2016 Application of plastic-damage multidirectional fixed smeared crack model in analysis of RC structures *Eng. Struct.* **125** 374–91
- [22] Cornelissen H A W, Hordijk D A and Reinhardt H W 1986 Experimental determination of crack softening characteristics of normalweight and lightweight concrete *HERON, Fract. Mech. Struct. Asp. Concr.* **31** 45–56
- [23] Coelho M R F 2017 *Bond behaviour of NSM FRP systems in concrete* (University of Minho)
- [24] Angelillo M, Lourenço P B and Milani G 2014 Masonry behaviour and modelling *Mechanics of Masonry Structures* ed M Angelillo (Springer Vienna)
- [25] RILEM TCS 1985 Determination of the fracture energy of mortar and concrete by means of three-point bend tests on notched beams *Mater. Struct.* **18** 287–90
- [26] American Society for Testing and Materials 2002 E 519-02 Standard test method for diagonal tension (shear) in masonry assemblages